J. Fluid Mech. (1965), *vol.* 22, *part* 2, *pp.* 285–304
Printed in Great Britain

A three-dimensional turbulent boundary layer

By A. E. PERRY AND P. N. JOUBERT
Department of Mechanical Engineering, University of Melbourne

(*Received* 26 *October* 1964)

The purpose of this paper is to provide some possible explanations for certain observed phenomena associated with the mean-velocity profile of a turbulent boundary layer which undergoes a rapid yawing. For the cases considered the yawing is caused by an obstruction attached to the wall upon which the boundary layer is developing. Only incompressible flow is considered.

§1 of the paper is concerned with the outer region of the boundary layer and deals with a phenomenon observed by Johnston (1960) who described it with his triangular model for the polar plot of the velocity distribution. This was also observed by Hornung & Joubert (1963). It is shown here by a first-approximation analysis that such a behaviour is mainly a consequence of the geometry of the apparatus used. The analysis also indicates that, for these geometries, the outer part of the boundary-layer profile can be described by a single vector-similarity defect law rather than the vector 'wall-wake' model proposed by Coles (1956). The former model agrees well with the experimental results of Hornung & Joubert.

In §2, the flow close to the wall is considered. Treating this region as an equilibrium layer and using similarity arguments, a three-dimensional version of the 'law of the wall' is derived. This relates the mean-velocity-vector distribution with the pressure-gradient vector and wall-shear-stress vector and explains how the profile skews near the wall. The theory is compared with Hornung & Joubert's experimental results. However at this stage the results are inconclusive because of the lack of a sufficient number of measured quantities.

1. Outer flow

Introduction

Johnston (1960) plotted his experimental velocity profiles for a yawed boundary layer in polar form. At a given position along the wall, the velocity vectors measured at various heights above the wall were drawn on a plane parallel to the wall from a single pole. He found that the vectors corresponding to the outer 90 % of the layer have their tips falling on one straight line. Hornung & Joubert (1963) carried out a more detailed experimental investigation of this phenomenon by yawing the boundary layer on a flat plate by a pressure field introduced by a circular cylinder standing on the plate. A typical plot of the velocity vectors is shown in figure 1, and it is seen that the triangular model of Johnston is confirmed by the experimental results. This can be given an interesting physical interpretation. Relative to an observer who rides with the flow in the free stream, the outer part of the velocity profile in the yawed boundary layer lies in one plane

and this plane slips sideways and rotates relative to the wall. It is as if the outer flow can be represented by a two dimensional profile which rides and turns on top of a thin sublayer which separates this outer region from the wall.

One would expect that such a phenomenon could be explained by examining some general properties of turbulent boundary layers. However, it is shown here that it is probably a consequency of the geometry of the apparatus used by Johnston and Hornung & Joubert.

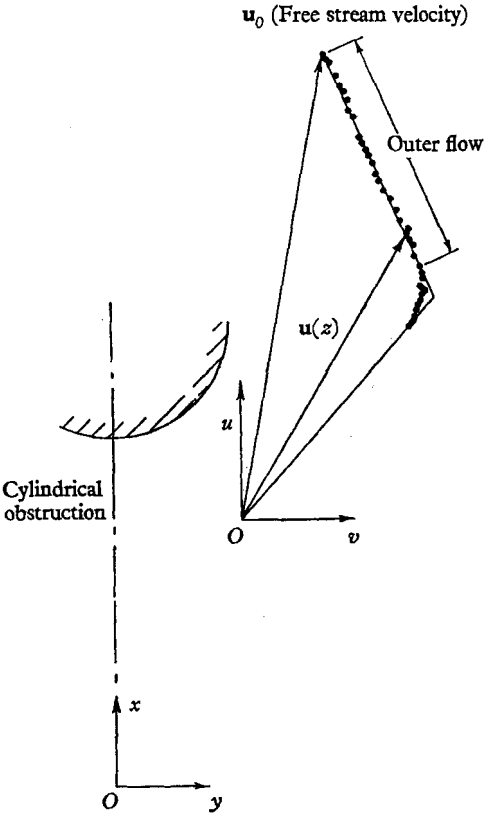

FIGURE 1. Typical Johnston plot as measured by Hornung & Joubert. z is measured normal to the wall.

Coles (1956) proposed that two-dimensional turbulent boundary layers have profiles which are expressible by the linear combination of two laws

$$u/u_\tau = f(zu_\tau/\nu) + \pi\omega(z/\delta),$$

where u is a velocity at distance z from the wall, u_τ is the friction velocity, ν is the kinematic viscosity, δ is the boundary-layer thickness, and π is a factor dependent on the upstream pressure gradient and wall-shear-stress distribution. The functions f and ω are universal, these being the 'law of the wall' and 'law of the wake' respectively. This agreed well with experiment and Coles suggested from intuitive arguments that for three-dimensional layers, the expression could be modified to read $\mathbf{u}/u_\tau = \mathbf{f}(zu_\tau/\nu) + \pi\omega(z/\delta)$,

where $\mathbf{f}$ is a vector which is in the direction of the wall shear stress and $\boldsymbol{\pi}$ is a vector such that $\mathbf{f}(\delta u_\tau/\nu)+\boldsymbol{\pi}\omega(1)$ is in the direction of the free-stream velocity $\mathbf{u}_0$. The value of $\boldsymbol{\pi}$ depends on the pressure and wall-shear-stress field.

This law did not apply to the experimental results of Hornung & Joubert. If the undisturbed upstream-velocity profile is two-dimensional, then, for the flow configurations tested, it is shown that Coles' equation should be replaced by

$$\frac{\mathbf{u}_0-\mathbf{u}}{u_\tau}=\boldsymbol{\Pi}\,\phi(z/\delta),$$

where $\phi(z/\delta)$ is the velocity-defect distribution of the undisturbed upstream-boundary-layer profile (divided by the local shear velocity). The vector $\boldsymbol{\Pi}$ depends on the pressure field and wall-shear-stress field, and some features of this dependence are indicated.

The experimental results of Hornung & Joubert are the most detailed to date and will be used exclusively in this paper except when stated otherwise.

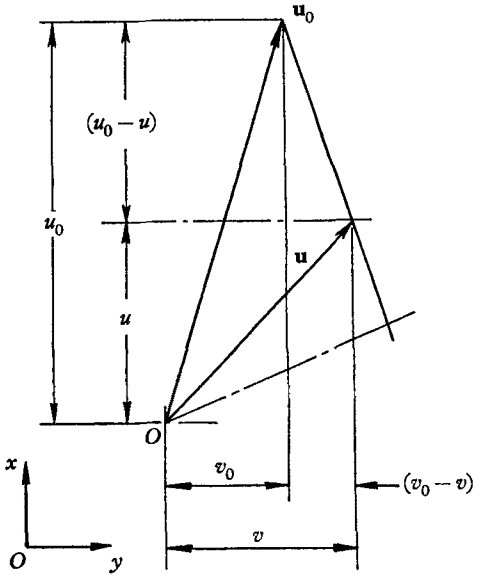

FIGURE 2. Analysis of Johnston plot.

Analysis

The analysis applies for flow configurations similar to those used by Johnston and Hornung & Joubert. All the necessary nomenclature is defined in figures 2 and 3. From figure 2 it can be seen that the Johnston triangle is valid so long as the ratio $(u_0-u)/(v_0-v)$ is independent of z, the distance from the wall. The aim of this analysis is to show that $(u_0-u)/(v_0-v)$ is a function of x and y alone for the flow configuration shown in figure 3.

In this figure it is shown where the streamlines of a typical yawed profile originate. The following assumptions are made:

(*a*) The approaching velocity profile is unaffected until it is fairly close to the cylinder. This means that the yawing is sudden and therefore the mean-flow

inertia and pressure-gradient forces predominate over most of the boundary-layer thickness. Therefore the total head along a mean streamline will be approximately constant for the relatively short length of streamlines considered.

(*b*) The approaching velocity profile is two-dimensional.

(*c*) The main effect of the obstacle is to yaw the boundary layer sideways and not to thicken it appreciably. The distance over which yawing occurs is small compared with the length required to produce the approaching two-dimensional

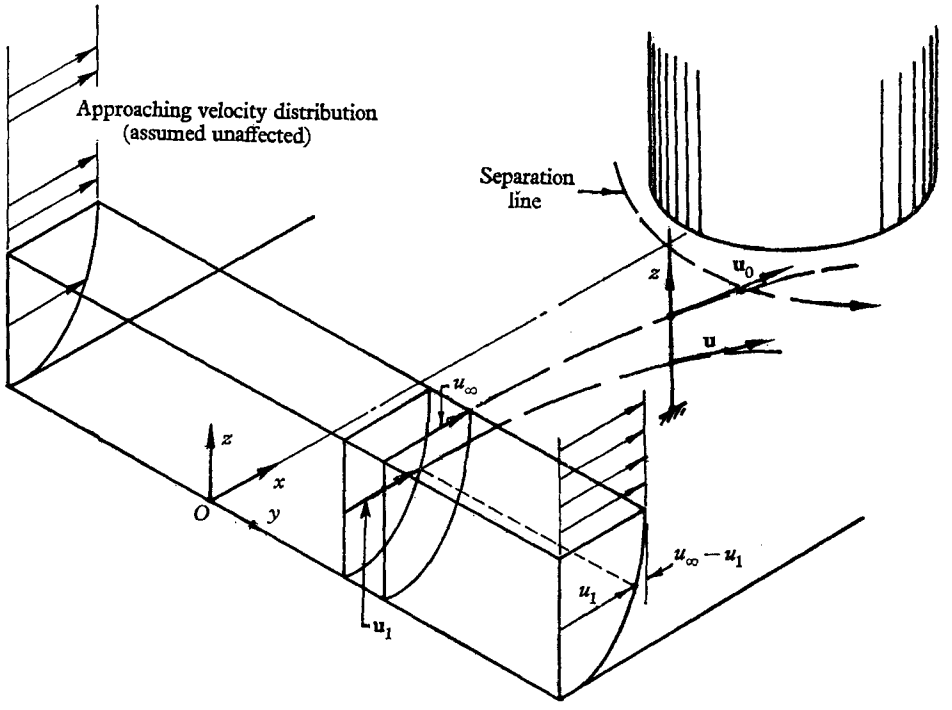

FIGURE 3. Geometry of system.

boundary layer, and so entrainment of irrotational fluid into the top of the layer in the yawing region will be relatively small. With two-dimensional boundary layers, rapid thickening of the layers occurs in regions of rising pressure mainly because there is a rapid build up of slower moving fluid close to the wall. In three-dimensional layers this fluid is free to escape sideways giving another reason for only small changes in δ. This agrees with experiment. The above argument also implies that the vertical component of velocity ω will be unusually small and this agrees with the smoke-tunnel observations of Schwind (1962).

The equations of motion for the mean-velocity field (neglecting shear stresses) are

$$u\frac{\partial u}{\partial x}+v\frac{\partial u}{\partial y}+w\frac{\partial u}{\partial z}=-\frac{1}{\rho}\frac{\partial p}{\partial x},$$

$$u\frac{\partial v}{\partial x}+v\frac{\partial v}{\partial y}+w\frac{\partial v}{\partial z}=-\frac{1}{\rho}\frac{\partial p}{\partial y},$$

$$u\frac{\partial w}{\partial x}+v\frac{\partial w}{\partial y}+w\frac{\partial w}{\partial z}=-\frac{1}{\rho}\frac{\partial p}{\partial z},$$

$$\frac{\partial u}{\partial x}+\frac{\partial v}{\partial y}+\frac{\partial w}{\partial z}=0.$$

Let the order of magnitude of changes in x and y be L and z be δ and the order of magnitude of u and v be U in the region yawing. Using the usual boundary-layer approximation that $\delta \ll L$ (experiments indicate that this could be about 0·1) the first two momentum equations have terms of order U^2/L while the third equation has terms of order $(U^2/L)(\delta/L)$. The equations reduce to

$$u\frac{\partial u}{\partial x}+v\frac{\partial u}{\partial y}+w\frac{\partial u}{\partial z}=-\frac{1}{\rho}\frac{\partial p}{\partial x}(x,y),$$

$$u\frac{\partial v}{\partial x}+v\frac{\partial v}{\partial y}+w\frac{\partial v}{\partial z}=-\frac{1}{\rho}\frac{\partial p}{\partial y}(x,y),$$

$$\frac{\partial u}{\partial x}+\frac{\partial v}{\partial y}+\frac{\partial w}{\partial z}=0,$$

i.e. p is not a function of z. This result was confirmed by experiment.

If only the outer region of the profiles is considered, it will be found that the velocity gradient $\partial u/\partial z$ will not be of order (U/δ), as in classical laminar-boundary-layer theory, but should really be of order (U/L) for the experiments considered. In turbulent boundary layers, it is usual for the velocity defect to remain small above a value of z/δ equal to about $\frac{1}{4}$ to $\frac{1}{3}$. The analysis will be restricted to this region, and as a first approximation the velocity defect will be assumed small, i.e. $u_1-u/u_0 \ll 1$. Using this approximation, and the fact that w is small (of order $U\delta/L$ by usual boundary-layer theory, but perhaps somewhat less because of assumption (*c*)), an order of magnitude analysis shows that the equations simplify to

$$u\frac{\partial u}{\partial x}+v\frac{\partial u}{\partial y}=-\frac{1}{\rho}\frac{\partial p}{\partial x}(x,y),$$

$$u\frac{\partial v}{\partial x}+v\frac{\partial v}{\partial y}=-\frac{1}{\rho}\frac{\partial p}{\partial y}(x,y),$$

$$\frac{\partial u}{\partial x}+\frac{\partial v}{\partial y}+\frac{\partial w}{\partial z}=0.$$

The pressure gradients will be those given by the free-stream velocity distribution $u_0(x,y)$ and $v_0(x,y)$, and so

$$u\frac{\partial u}{\partial x}+v\frac{\partial u}{\partial y}=u_0\frac{\partial u_0}{\partial x}+v_0\frac{\partial u_0}{\partial y}, \tag{1}$$

$$u\frac{\partial v}{\partial x}+v\frac{\partial v}{\partial y}=u_0\frac{\partial v_0}{\partial x}+v_0\frac{\partial v_0}{\partial y}, \tag{2}$$

$$\frac{\partial u}{\partial x}+\frac{\partial v}{\partial y}+\frac{\partial w}{\partial z}=0. \tag{3}$$

Thus there are three equations and three unknowns, these being u, v and w. Equations (1) and (2) are all that is necessary for determining u and v (except

for the boundary conditions), while equation (3) can be used for finding w once u and v are known. Equations (1) and (2) can be re-expressed in terms of the velocity defects $\Delta u = u_0 - u$ and $\Delta v = v_0 - v$; thus

$$\Delta u\frac{\partial \Delta u}{\partial x} + \Delta v\frac{\partial \Delta u}{\partial y} = \Delta u\frac{\partial u_0}{\partial x} + \Delta v\frac{\partial u_0}{\partial y} + u_0\frac{\partial \Delta u}{\partial x} + v_0\frac{\partial \Delta u}{\partial y}, \tag{4}$$

$$\Delta u\frac{\partial \Delta v}{\partial x} + \Delta v\frac{\partial \Delta v}{\partial y} = \Delta u\frac{\partial v_0}{\partial x} + \Delta v\frac{\partial v_0}{\partial y} + u_0\frac{\partial \Delta v}{\partial x} + v_0\frac{\partial \Delta v}{\partial y}. \tag{5}$$

Since the analysis is restricted to small velocity defects, all predominant terms will be contained on the right-hand side of these equations. It has been indicated that experiment shows that $\Delta u/\delta = O(U/L)$, and an order of magnitude argument shows that the equations become

$$\Delta u\frac{\partial u_0}{\partial x} + \Delta v\frac{\partial u_0}{\partial y} + u_0\frac{\partial \Delta u}{\partial x} + v_0\frac{\partial \Delta u}{\partial y} = 0, \tag{6}$$

$$\Delta u\frac{\partial v_0}{\partial x} + \Delta v\frac{\partial v_0}{\partial y} + u_0\frac{\partial \Delta v}{\partial x} + v_0\frac{\partial \Delta v}{\partial y} = 0. \tag{7}$$

If, for a given value of z, the initial velocity defect is $\Delta u_1 = u_\infty - u_1$ at the upstream reference profile (see figure 3), then these equations become after non-dimensionalizing with Δu_1

$$\Delta u^*\frac{\partial u_0}{\partial x} + \Delta v^*\frac{\partial u_0}{\partial y} + u_0\frac{\partial \Delta u^*}{\partial x} + v_0\frac{\partial \Delta u^*}{\partial y} = 0, \tag{8}$$

$$\Delta u^*\frac{\partial v_0}{\partial x} + \Delta v^*\frac{\partial v_0}{\partial y} + u_0\frac{\partial \Delta v^*}{\partial x} + v_0\frac{\partial \Delta v^*}{\partial y} = 0, \tag{9}$$

where $\Delta u^* = \Delta u/\Delta u_1$ and $\Delta v^* = \Delta v/\Delta u_1$.

The boundary conditions for a given value of Z are

$$\left.\begin{aligned} &\Delta u^* = 1 \quad \text{at} \quad x = 0, \\ \text{and} \quad &\Delta v^* = 0 \quad \text{at} \quad x = 0 \quad \text{and} \quad y = 0. \end{aligned}\right\} \tag{10}$$

The quantities u_0, v_0, $\partial u_0/\partial x$, $\partial u_0/\partial y$, $\partial v_0/\partial x$ and $\partial v_0/\partial y$ are prescribed by the free-stream flow, which is independent of the boundary-layer behaviour. Therefore all necessary information for finding Δu^* and Δv^* (equations (8), (9) and (10)) are independent of z, and so Δu^* and Δv^* are independent of z. Hence, as a first approximation, the equations of motion indicate that the Johnston triangle is valid.† It will be noted that the validity of the Johnston triangle depends on the linearity of (6) and (7) with respect to Δu and Δv.

The above analysis also indicates that since Δu^* and Δv^* are independent of z then

$$\mathbf{u}_0 - \mathbf{u} = (u_\infty - u_1)\,\mathbf{\Pi}'(x, y) \tag{11}$$

for the same value of z, where $\mathbf{\Pi}'(x, y)$ is a vector depending on the free-stream flow and is independent of the conditions at the wall or the shape of the initial upstream profile. Since slight boundary-layer thickening probably occurs at places where the streamline in the boundary layer diverged from the wall, then

† If the approximation used in reducing equations (4) and (5) to (6) and (7) had not been used, this deduction could not have been made.

as a first approximation, streamlines could be regarded as having a constant value of z/δ. The effect of the vertical velocity can then perhaps be partly accounted for by applying equations (8) and (9) to surfaces of constant values of z/δ, which will be approximately plane, but at a slight angle to the wall. Therefore an

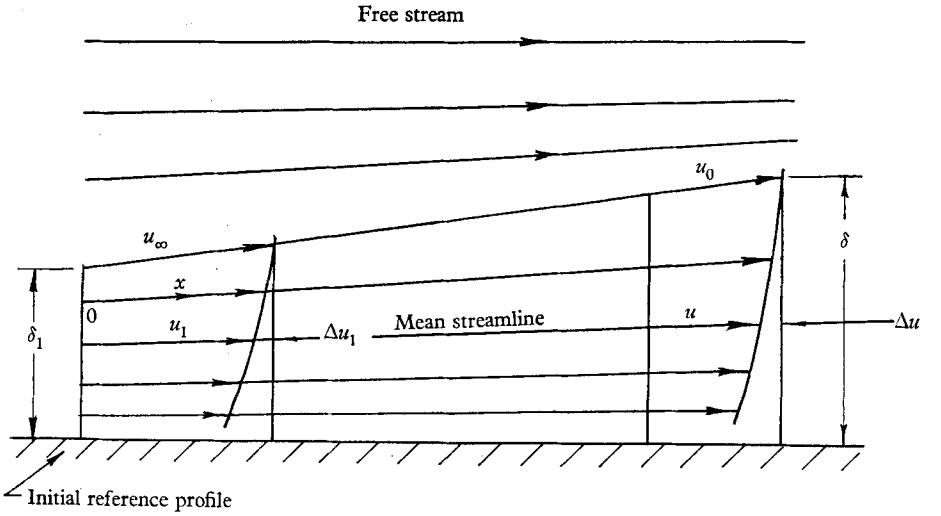

FIGURE 4. Assumed flow on plane of symmetry. The entrainment of fluid into the boundary layer is considered to be small. Total head along the mean streamline is equal to a constant (equations (4) and (5)); also as a first approximation to improve the theory z/δ along the mean streamline is assumed constant.

improved approximation would be to say that equation (11) is applicable for the same values of z/δ providing the boundary-layer thickening was slight (this is illustrated in figure 4). That is

$$\mathbf{u}_0 - \mathbf{u} = \mathbf{\Pi}'(x,y)\,\phi'(z/\delta), \quad \text{where} \quad \phi'(z/\delta) = u_\infty - u_1,$$

or

$$\frac{\mathbf{u}_0 - \mathbf{u}}{u_\tau} = \mathbf{\Pi}(x,y)\,\phi(z/\delta), \quad \text{where} \quad \phi(z/\delta) = \frac{u_\infty - u_1}{u_{\tau_1}}. \tag{12}$$

u_{τ_1} is the shear velocity appropriate to the upstream reference profile, and u_τ is the local shear velocity. $\mathbf{\Pi}(x,y)$ is a factor somewhat analogous to the factor used by Coles in his 'law of the wake' model mentioned in the introduction.

Discussion of results

To illustrate the validity of equation (11), the velocity defects were plotted against one another for the same values of z (δ was fairly constant). Straight lines should be produced for small velocity defects. It can be seen from these plots (figure 5) and from the Johnston triangles, that the theory seems to be applicable for a much greater range of defects than was expected. The theory seems quite satisfactory, even for values of $\Delta u/u_0$ as large as 0·4. This is partially explained by considering the solution to the equations for the simple case of flow along the plane of symmetry (see figure 4).

For this case, equations (4) and (5) for a given value of (z/δ) reduce to

$$\left\{\left(\frac{\Delta u_1}{u_\infty}\right)^2 - 2\left(\frac{\Delta u_1}{u_\infty}\right)\right\} = \left(\frac{u_0}{u_\infty}\right)^2 \left\{\left(\frac{\Delta u}{u_0}\right)^2 - 2\left(\frac{\Delta u}{u_0}\right)\right\}. \tag{13}$$

Making the approximation in reducing equations (4) and (5) to equations (6) and (7), the above equation becomes

$$\lim_{\Delta u_1 \to 0} \frac{\Delta u}{\Delta u_1} = \frac{u_\infty}{u_0}. \tag{14}$$

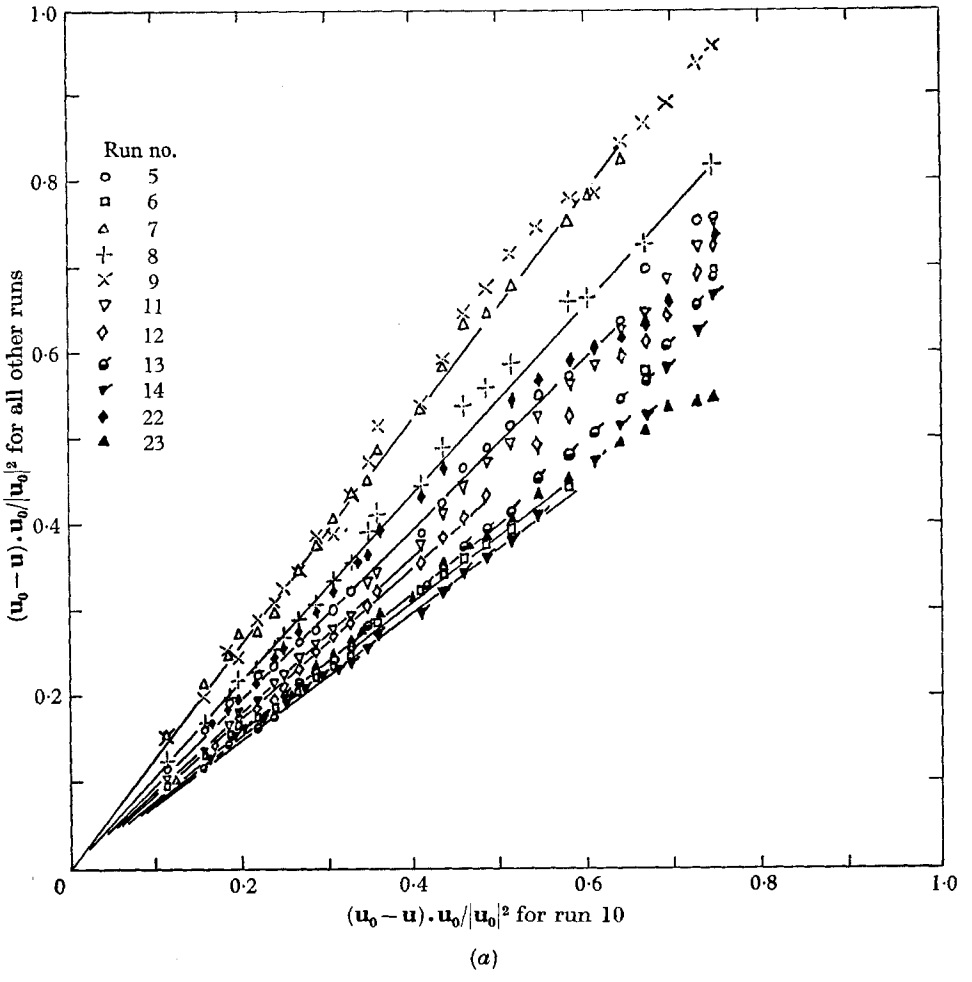

FIGURE 5. Comparison of velocity defects for same values of z. (*a*) Profiles upstream of the separation line; (*b*) downstream profiles (theory not applicable since ω is large).

$\Delta u/\Delta u_1$ has been calculated for a typical upstream profile in the tests of Hornung & Joubert for various pressure coefficients $C_p = (u_\infty^2 - u_0^2)/u_\infty^2$ using both equations (13) and (14). For these tests, $C_p \doteqdot 0{\cdot}3$ max. before separation was reached, and the percentage error in using equation (14) is only about 15 % where

$$\Delta u_1/u_\infty = 0{\cdot}390 \quad \text{and} \quad z/\delta = \tfrac{1}{8}.$$

For flow further from the wall and for smaller C_p, the error is much less. The results of these calculations are shown in figure 6. This looks very promising, but a complete numerical solution to equations (8) and (9) is really required. As yet this has not been done.

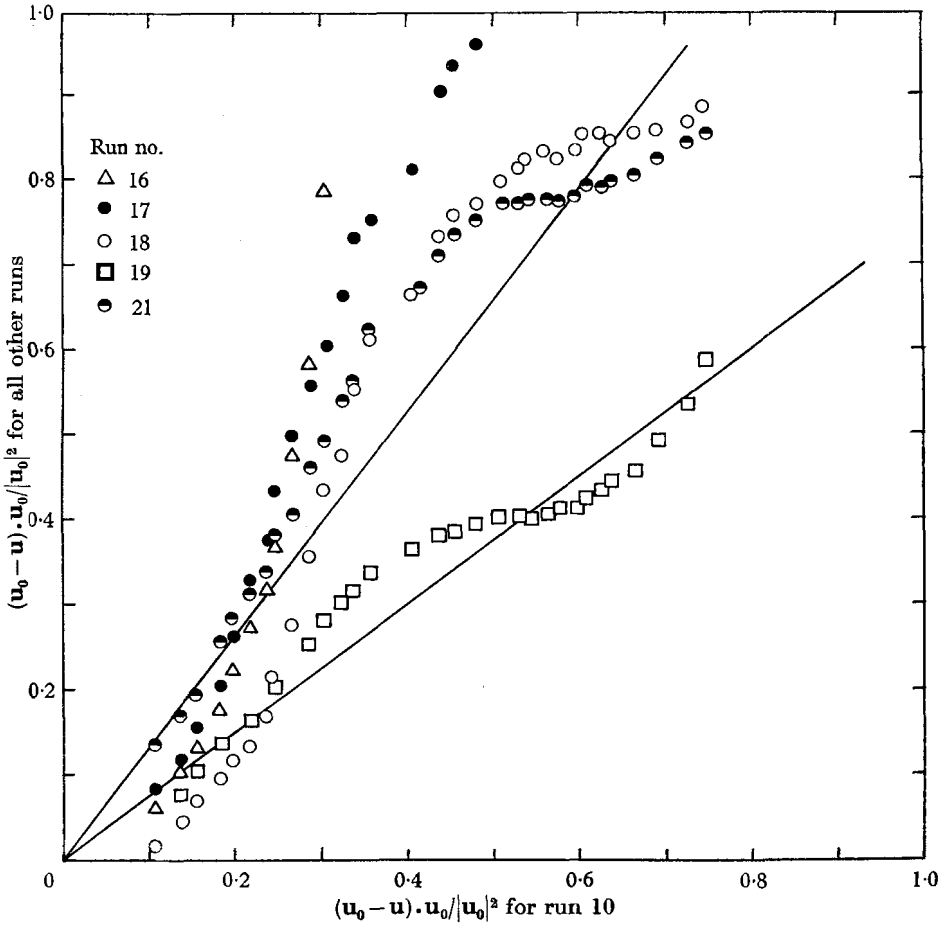

(*b*)

For legend see facing page.

2. Inner flow

Introduction

Hornung & Joubert proposed that the 'law of the wall' applies to three-dimensional boundary layers in the same form as it does to two-dimensional layers up to the point where the boundary layer becomes yawed. This probably means that the law is applicable up to the apex of the Johnston triangle which has a value of zu_τ/ν which ranges up to 150. The velocities are found to be close to the wall-shear-stress direction up to this point. The experimental results for this law of the wall are shown in figure 7 for the various experimental runs. However, the law is not conclusive since direct measurements of shear stress were not carried out. Also only a few points from each run fall on the proposed curve.

The values of the shear stress or local skin-friction coefficient were determined by plotting the magnitude of $|\mathbf{u}|/|\mathbf{u}_0|$ ($\mathbf{u}_0$ being the local free-stream velocity) against $\log(z|\mathbf{u}_0|/\nu)$, that is on a Clauser chart (Clauser 1954). Assuming that the

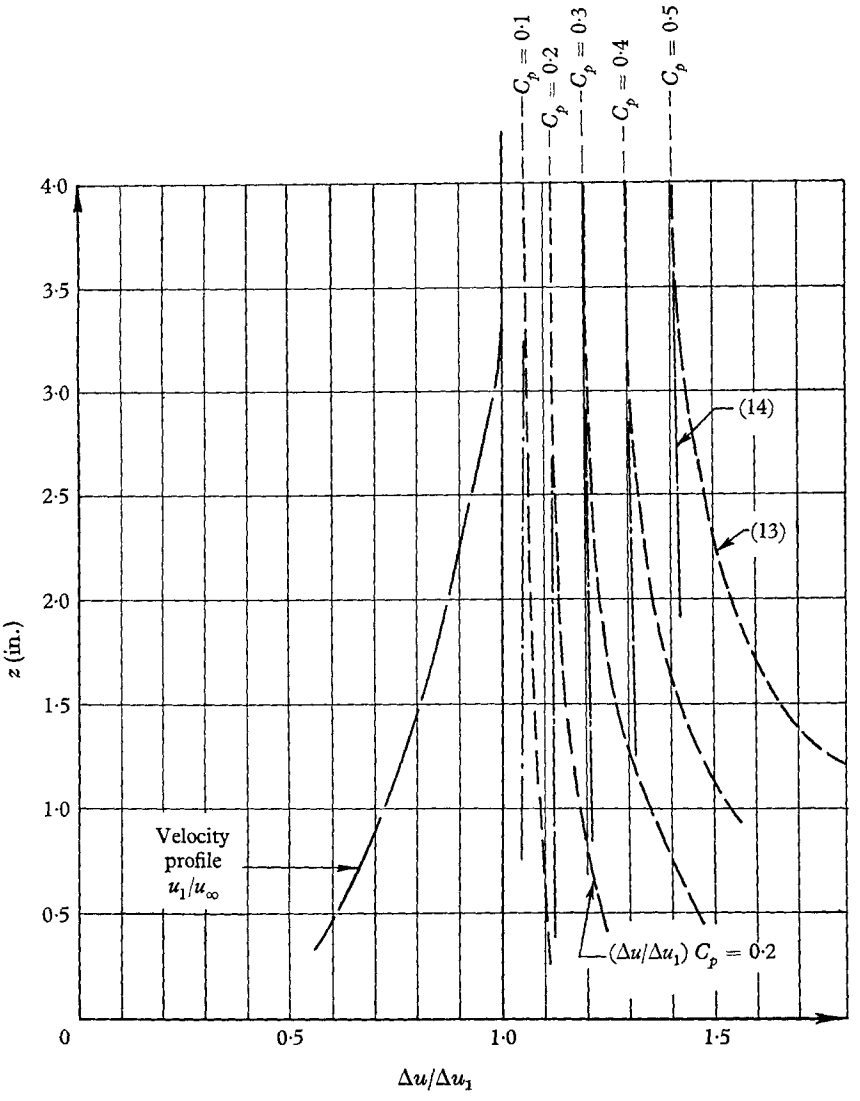

FIGURE 6. Comparison of equations (14) and (13).

usual law of the wall is applicable, then such a chart consists of a family of straight lines, each line corresponding to a different value of the local skin friction coefficient C_f'. The equation of each line is

$$\frac{|\mathbf{u}|}{|\mathbf{u}_0|} = 5{\cdot}6\sqrt{\frac{C_f'}{2}}\log_{10}\left\{\frac{z|\mathbf{u}_0|}{\nu}\right\} + \sqrt{\frac{C_f'}{2}}\left\{5{\cdot}6\log_{10}\sqrt{\frac{C_f'}{2}} + 4{\cdot}9\right\}$$

and is illustrated in figure 8. $C_f' = \tau_0/(\frac{1}{2}\rho|\mathbf{u}_0|^2)$, where τ_0 is the wall shear stress.

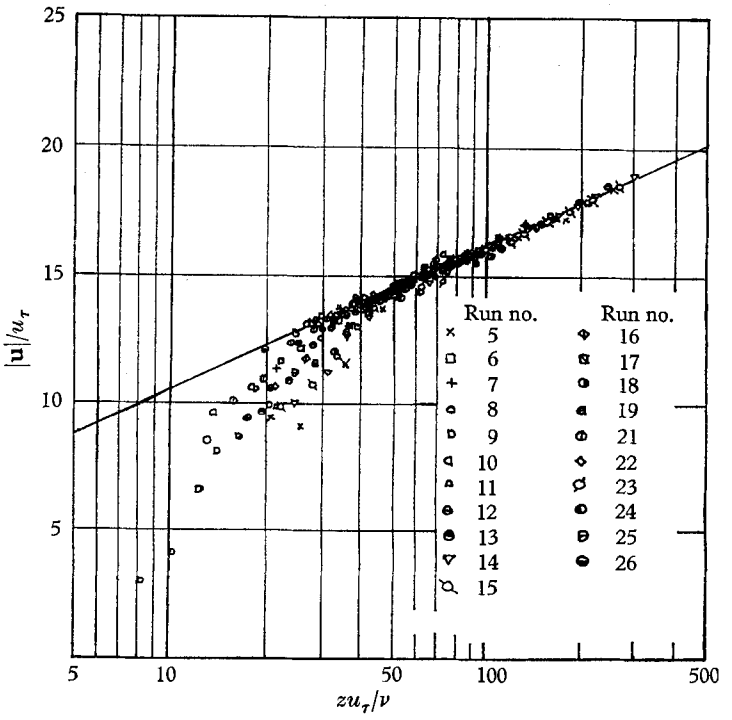

FIGURE 7. The law of the wall of Hornung & Joubert.

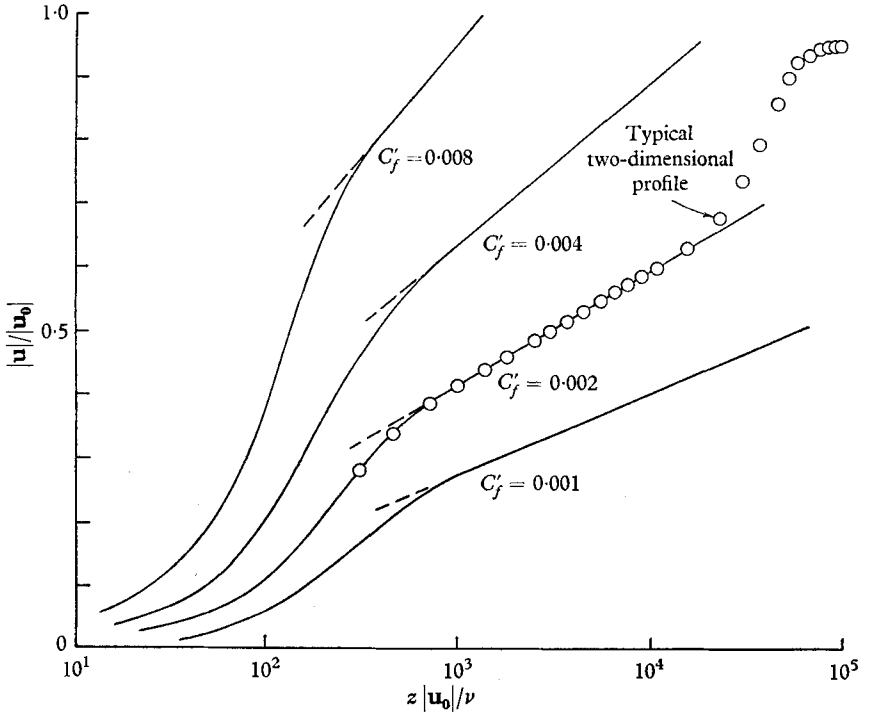

FIGURE 8. Determining C_f' for smooth surfaces using Clauser's chart.

If this law of the wall is applicable for three-dimensional turbulent boundary layers, then the experimental points displayed on such a chart should fit into this 'Clauser scheme', i.e. the points should lie on lines whose slope and position obviously fit into the above pattern. However, the slope of the experimental lines could not be accurately relied on because of the lack of the number of points forming a straight line. C_f' was therefore assumed to be that value indicated only by the position of the points.

One reason for this lack of range of semi-logarithmic profile may be due to the yawing effect of the boundary layer, which really occurs well before the apex of the Johnston triangle.

Analysis

As a first step to improve the correlation of results, the following theory is proposed.

Since the familiar law of the wall

$$\frac{u}{u_\tau} = \frac{1}{k}\ln\left(\frac{zu_\tau}{\nu}\right) + A$$

found for two-dimensional boundary layers can be arrived at from various phenomenological theories, which invariably end up by integration of a differential equation of the form

$$\frac{\tau}{\rho} = \epsilon\frac{\partial u}{\partial z} \doteqdot \frac{\tau_0}{\rho},$$

then perhaps a three-dimensional law of the wall can be arrived at by an appropriate three-dimensional interpretation of the terms in this equation. The term $\partial u/\partial z$ is actually a rate of strain, and the shear-stress τ will be assumed to act in a direction of the maximum rate of strain. By looking at a Johnston plot, the maximum rate of strain will occur along lines tangent to the curve described by the tips of the velocity vectors.

As a first tentative approximation, it is assumed that the magnitude of the shear-stress 'vector' (which lies in the same direction as the maximum strain rate) is constant, and that the eddy viscosity $\epsilon = kz(\tau_0/\rho)^{\frac{1}{2}}$ as it is for two-dimensional layers. Integration leads to

$$\frac{u}{u_\tau} = \frac{1}{k}\ln\left(\frac{zu_\tau}{\nu}\right) + A,$$

provided u in this case is not the magnitude of velocity, but rather the length of arc on the curve of the Johnston plot. That is, the 'developed' velocity distribution should be used. This point is amplified later. This arc length will be written as U.

The above technique of plotting the profiles was carried out on a number of experimental runs of Hornung & Joubert, and it was found that the curves straightened out to give a much greater range of semi-logarithmic lines. A typical comparison between a magnitude plot and 'developed' plot of the wall results is shown in figure 9, and it can be seen that this law appears now to be valid well beyond the apex of the Johnston triangle.

This looked encouraging and a number of such profiles of 'developed' $U/|\mathbf{u}_0|$ versus log $z|\mathbf{u}_0|/\nu$ were superimposed on the Clauser chart (see figure 10). However, it can be seen that the slope of the semi-logarithmic lines of best fit definitely do not fit into the Clauser scheme of things. It was first thought that these deviations may have been due to the effects of surface roughness. However,

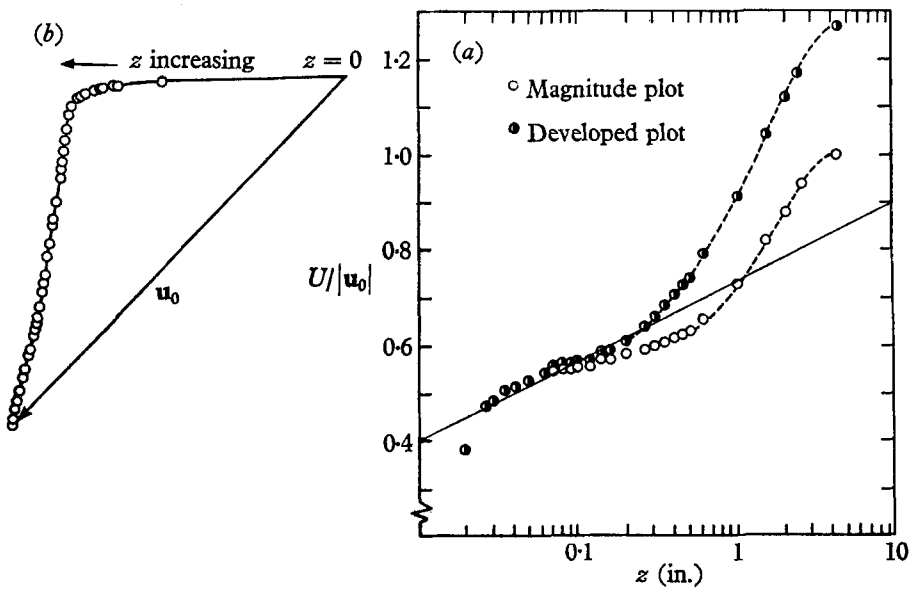

FIGURE 9. Run 22 of Hornung & Joubert. (*a*) Comparison of magnitude and developed plot; (*b*) Johnston plot.

using the techniques outlined by Perry & Joubert (1963) to determine the roughness function, negative values of this function were obtained for some profiles. This is not possible. The plate used by Hornung & Joubert may have had some slight roughening, but it appears that the answer lies in the proposition that the results do not really follow a semi-logarithmic law since pressure-gradient effects near the wall were strong. This possibility was borne out by a more general analysis which takes into account the pressure-gradient effects, and is as follows.

As in two-dimensional layers, mean-flow inertia forces close to the wall will be neglected so that there is a balance of pressure-gradient forces with shear-stress forces. The co-ordinate system used will be the same as in §1.

Consider a prismatic element of sides dx, dy, and dz at distance z from the wall. The shear-stress τ_{xy} acts in the x-direction on the (x,z)-face. Using this sign convection, equilibrium of forces on the element give the following equations

$$\frac{\partial p}{\partial x}+\frac{\partial \tau_{xy}}{\partial y}+\frac{\partial \tau_{xz}}{\partial z}=0, \quad \text{etc.},$$

$$\tau_{xy}=\tau_{yx}, \qquad \text{etc.}$$

To give the analysis a stronger theoretical backing, this layer close to the wall will be considered an equilibrium layer in the sense used by Townsend (1961),

who developed the concept for two-dimensional layers. He showed that, very close to the wall, the local production and dissipation of energy predominate over other forms of energy, and that the flow structure at a point depends mainly on local variables such as the local shear-stress τ and distance z from the wall. This

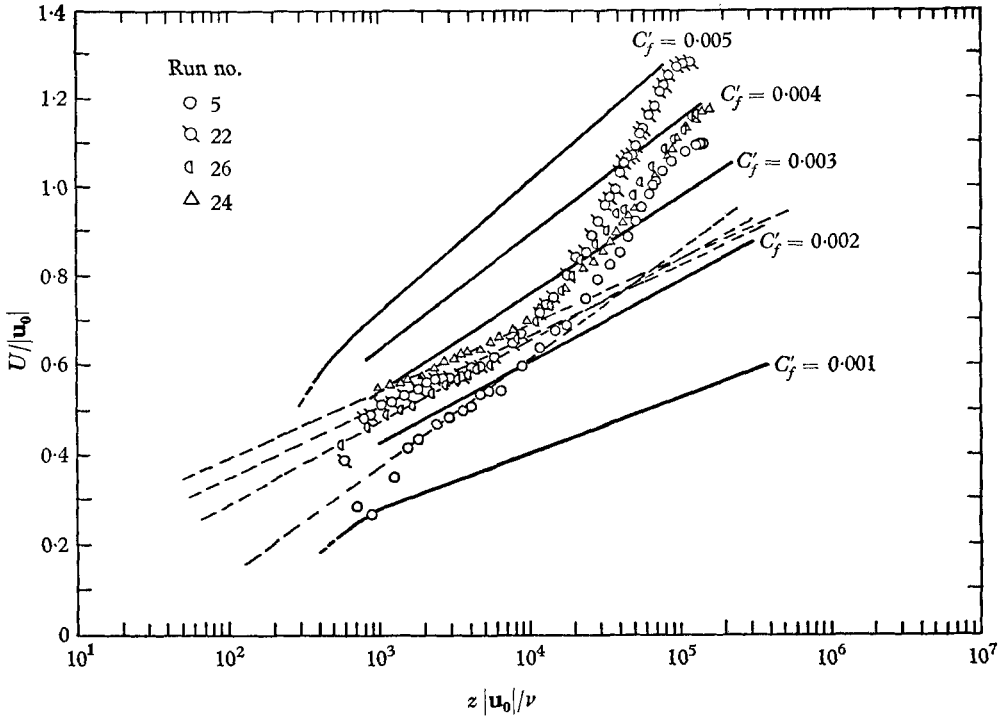

FIGURE 10. Comparison of 'developed' velocity profiles with the 'Clauser scheme'. ———, Clauser lines; – – –, semi-log lines of best fit.

led finally to the conclusion that a 'mixing-length' interpretation of the mean-flow energy equations was valid. Therefore the concept of eddy viscosity will be used, and the shear stresses will be assumed to be related to the strain rates by

$$\tau_{xy} = \rho\epsilon_1\left\{\frac{\partial u}{\partial y}+\frac{\partial v}{\partial x}\right\}, \quad \text{etc.}$$

Here ϵ_1, ϵ_2, and ϵ_3 are three components of an eddy-viscosity tensor.

Close to the wall, velocities vary very rapidly with z and the flow is nearly parallel to the wall (hence $w = 0$). Velocity variations with x and y will be considered to be small compared with the variations with z. Hence

$$\tau_{xy} = 0, \quad \tau_{xz} = \epsilon_2\rho\frac{du}{dz}, \quad \tau_{yz} = \epsilon_3\rho\frac{dv}{dz}. \tag{15}$$

The force-equilibrium equations become

$$\frac{\partial p}{\partial x} = -\frac{d\tau_{xz}}{dz}, \quad \frac{\partial p}{\partial y} = -\frac{d\tau_{yz}}{dz}.$$

Integration of these equations with respect to z, noting that $p = p(x, y)$, gives

$$\tau_{xz} = \tau_{xz_0} - z\frac{\partial p}{\partial x}, \quad \tau_{yz} = \tau_{yz_0} - z\frac{\partial p}{\partial y}. \tag{16}$$

The suffix 0 denotes conditions at the wall.

Equation (15) does not appear to be of much use since the relationship between ϵ_2 and ϵ_3 is not known. One could perhaps assume the eddy viscosity to be an isotropic tensor, and it seems reasonable to make the hypothesis indicated earlier, which states that the maximum shear stress acts in the same direction as the maximum strain rate. From Townsend's hypothesis for two-dimensional layers, the eddy viscosity connecting these two quantities will depend on the local maximum shear-stress, z and ρ.

Hence, perhaps for three-dimensional layers,

$$(\tau_{xz}^2 + \tau_{yz}^2)^{\frac{1}{2}} = \rho\epsilon\left\{\left(\frac{du}{dz}\right)^2 + \left(\frac{dv}{dz}\right)^2\right\}^{\frac{1}{2}}, \tag{17}$$

and ϵ is given by dimensional reasoning as

$$\epsilon = k\rho^{-\frac{1}{2}}(\tau_{xz}^2 + \tau_{yz}^2)^{\frac{1}{4}} z.$$

$(\tau_{xz}^2 + \tau_{yz}^2)^{\frac{1}{2}}$ and $\{(du/dz)^2 + (dv/dz)^2\}^{\frac{1}{2}}$ are the maximum shear-stress and strain-rate magnitudes respectively, and k is a universal constant.

Equation (17) becomes

$$(\tau_{xz}^2 + \tau_{yz}^2)^{\frac{1}{2}} = \rho^{\frac{1}{2}} kz\left\{\left(\frac{du}{dz}\right)^2 + \left(\frac{dv}{dz}\right)^2\right\}^{\frac{1}{2}}. \tag{18}$$

Substituting equation (16) into (18) gives

$$\left\{\tau_{xz_0}^2 + \tau_{yz_0}^2 - 2z\tau_{xz_0}\frac{\partial p}{\partial x} - 2z\tau_{yz_0}\frac{\partial p}{\partial y} + z^2\left(\frac{\partial p}{\partial x}\right)^2 + z^2\left(\frac{\partial p}{\partial y}\right)^2\right\}^{\frac{1}{2}} = \rho^{\frac{1}{2}} kz\left\{\left(\frac{du}{dz}\right)^2 + \left(\frac{dv}{dz}\right)^2\right\}^{\frac{1}{2}}. \tag{19}$$

$(\tau_{xz_0}^2 + \tau_{yz_0}^2)^{\frac{1}{2}}$ (which will be written as τ_0) is the magnitude of a vector $\boldsymbol{\tau}_0$, the shear stress at the wall, while $\{(\partial p/\partial x)^2 + (\partial p/\partial y)^2\}^{\frac{1}{2}}$ (which will be written as $\rho\alpha$) is the magnitude of a pressure-gradient vector $\rho\boldsymbol{\alpha}$. $\tau_{xz_0}(\partial p/\partial x) + \tau_{yz_0}(\partial p/\partial y)$ is obviously the scalar product of the two vectors $\rho\boldsymbol{\alpha}$ and $\boldsymbol{\tau}_0$ and will be written as $\tau_0\rho\alpha\cos\theta$ where θ is the angle between these vectors. Equation (19) therefore becomes

$$\{\tau_0^2 - 2z\tau_0\rho\alpha\cos\theta + z^2\alpha^2\}^{\frac{1}{2}} = \rho^{\frac{1}{2}} kz\left\{\left(\frac{du}{dz}\right)^2 + \left(\frac{dv}{dz}\right)^2\right\}^{\frac{1}{2}}.$$

Integrating the above equation and putting $zu_\tau/\nu = z^*$ leads to

$$\frac{U}{u_\tau} = \frac{\int\left\{1 + \left(\frac{dv}{du}\right)^2\right\}^{\frac{1}{2}} du}{u_\tau} = \frac{1}{k}\int\frac{1}{z^*}\left\{1 - 2\cos\theta\left(\frac{\alpha\nu}{u_\tau^3}\right)z^* + \left(\frac{\alpha\nu}{u_\tau^3}\right)^2 z^{*2}\right\}^{\frac{1}{4}} dz^*, \tag{20}$$

where $u_\tau = \sqrt{(\tau_0/\rho)}$.

The significant quantity in the expression for the law of the wall is therefore the length of arc on the Johnston plot. This verifies the intuitive assumption made earlier.

For small values of z^*, experimental results indicate that U is closely equal to the magnitude of the velocity vector, and the boundary condition suggested by Townsend† for his two-dimensional equilibrium layers will be used. That is

$$\lim_{z^*\to 0}\left(\frac{U}{u_\tau}\right) = \frac{1}{k}\ln z^* + A,$$

where A is a parameter influenced only by surface roughness effects and is constant for smooth walls.

Therefore

$$\frac{U}{u_\tau} = \frac{1}{k}\int_0^{z^*}\frac{1}{z^*}\left\{1 - 2\cos\theta\left(\frac{\alpha\nu}{u_\tau^3}\right)z^* + \left(\frac{\alpha\nu}{u_\tau^3}\right)^2 z^{*2}\right\}^{\frac{1}{2}} dz^* + A. \tag{21}$$

Some interesting results of this equation should be noted. For small values of $\alpha\nu/u_\tau^3$, the equation reduces to the simple semi-logarithmic profile and represents the case of a two-dimensional constant-stress layer. When $\theta = \pi$, equation (21) simplifies to

$$\frac{U}{u_\tau} = \frac{1}{k}\int_0^{z^*}\frac{1}{z^*}\left\{1 + \left(\frac{\alpha\nu}{u_\tau^3}\right)z^*\right\}^{\frac{1}{2}} dz^* + A,$$

which is equivalent to Townsend's two-dimensional linear stress layer in an adverse pressure gradient. With $\theta = 0$, the pressure gradient is favourable. For the case of the adverse pressure gradient, large values of z^* give

$$\frac{U}{u_\tau} = \frac{2}{k}\left(\frac{\alpha\nu}{u_\tau^3}\right)z^{*\frac{1}{2}},$$

the familiar half-power law of Townsend.‡ This case also serves to verify the correctness of the sign convections used for θ. The shear-stress vector $\boldsymbol{\tau}_0$ is that force per unit area acting on the wall. The pressure-gradient vector $\boldsymbol{\alpha}$ has the same sense as the force it produces on a fluid element, that is, in a sense opposite to ∇p. The angle θ is zero when $\boldsymbol{\tau}_0$ and $\boldsymbol{\alpha}$ act in the same sense.

Equation (21) is shown plotted in figure 11.

The effect of varying the parameter $\alpha\nu/u_\tau^3$ is to cause the deviations (shown heavy) from the semi-logarithmic line to shift bodily up and down along the line.

Range of validity of equation (21)

An idea of the maximum possible range of validity of equation (21) can be deduced from the Johnston plot. In figure 12, it is shown how the experimental points for the wall flow blend in with the straight side of the 'triangle' (which corresponds with the points for the outer flow). Consider a prismatic element measuring dx by dy and z_1 units high. The shear force acting on the bottom face

† Of course, physically $\lim_{z^*\to 0}(U/u_\tau) = z^*$ but this is in the region influenced by viscous effects, being outside the validity of equation (20).

‡ Energy conveyed by turbulent diffusive movements has been neglected here whereas Townsend took this into account by a small additional term.

$z = 0$ is assumed to act in the direction of the maximum strain rate at $z = 0$ while, at $z = z_1$, the appropriate direction is given by the tangent on the Johnston plot for $z = z_1$. These two directions are indicated by the dotted lines. The equilibrium of the prismatic element is shown by the force polygon in the figure. The sense of the shear-force vector is reversed at $z = z_1$ since the top face of the element is being considered. The resultant shear force is of course in the direction of $\boldsymbol{\alpha}$ since inertia forces have been neglected.

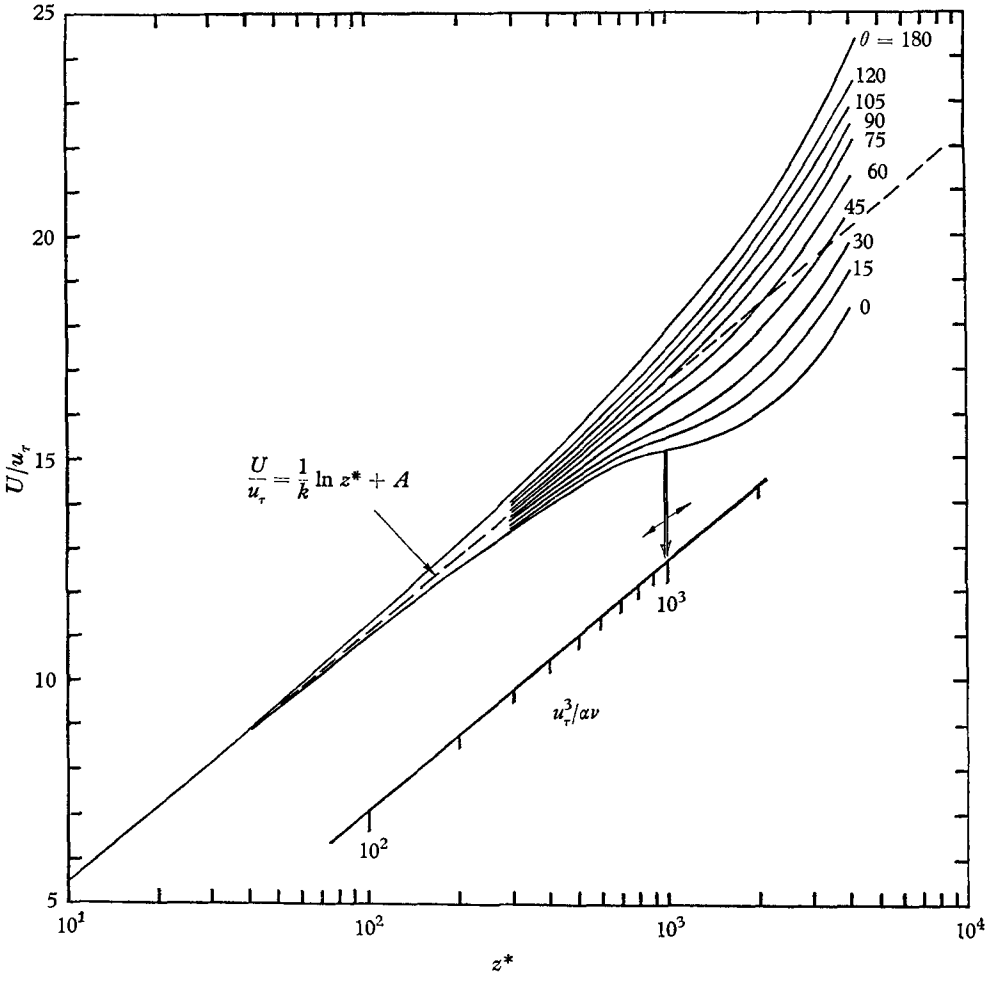

FIGURE 11. Three-dimensional law of the wall.

Once the straight side of the Johnston plot is reached ($z = z_2$), no further change in the direction of the shear-force $\tau_z dx dy$ can occur and so the force triangle will not close for values of z greater than z_2. Since z_2 is in the outer flow, the value of $\tau_z dx dy$ should be small and this requires τ_0 to have the same direction as $\boldsymbol{\alpha}$. Experiments indicate that this is in general far from the truth and mean-flow inertia forces probably come into play before z exceeds the values corre-

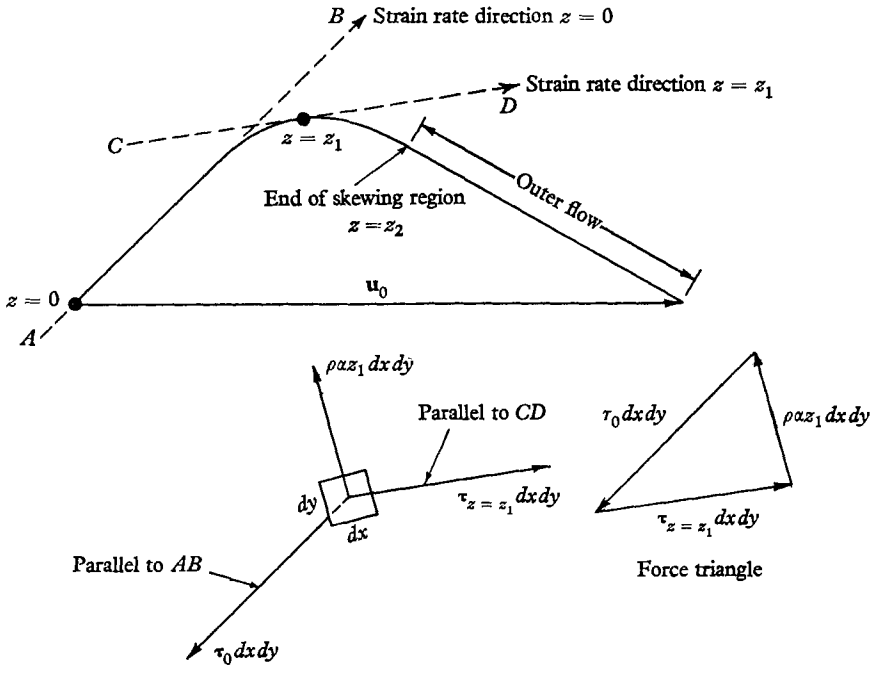

FIGURE 12. Equilibrium of fluid element.

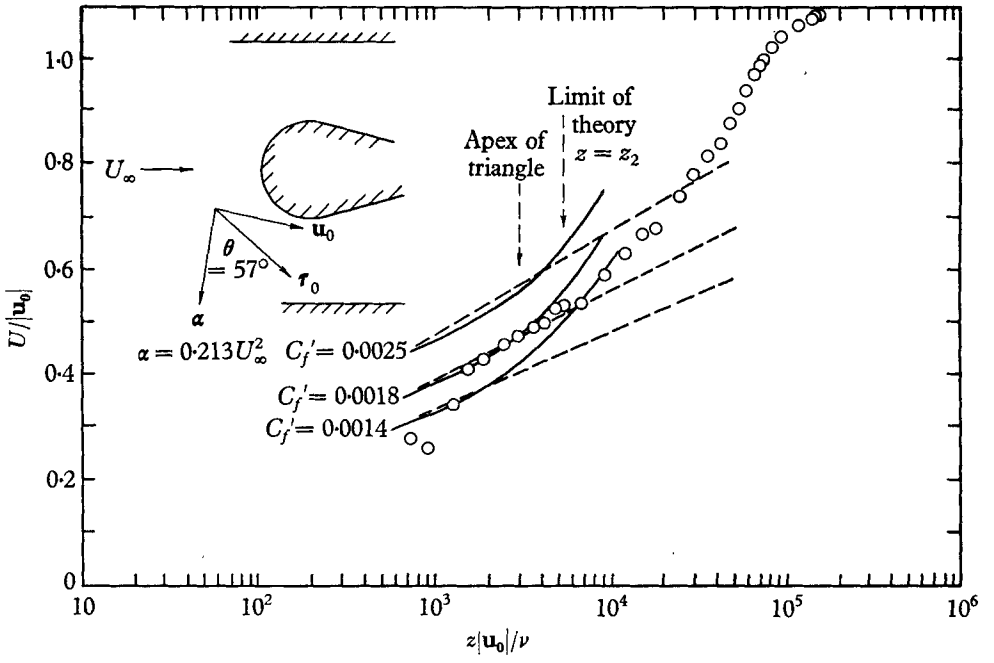

FIGURE 13. Comparison of run 5 with theory. ———, theory and interpolation; – – – –, Clauser lines.

sponding to the straight side of the Johnston plot. At best equation (21) cannot be valid for values of z outside the curved portion of the plot or what could be referred to as the 'skewing region'.

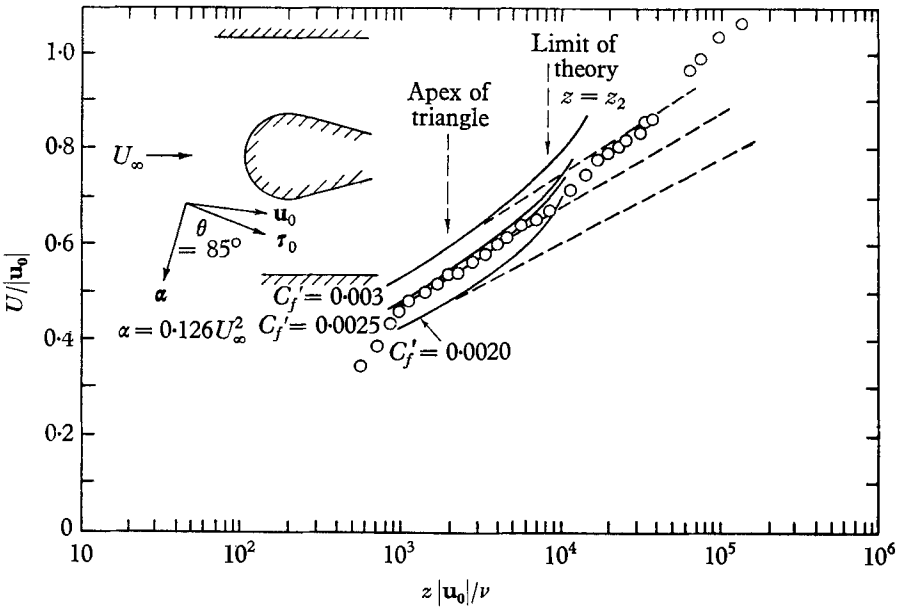

FIGURE 14. Comparison of run 14 with theory. ———, theory and interpolation; – – – –, Clauser lines.

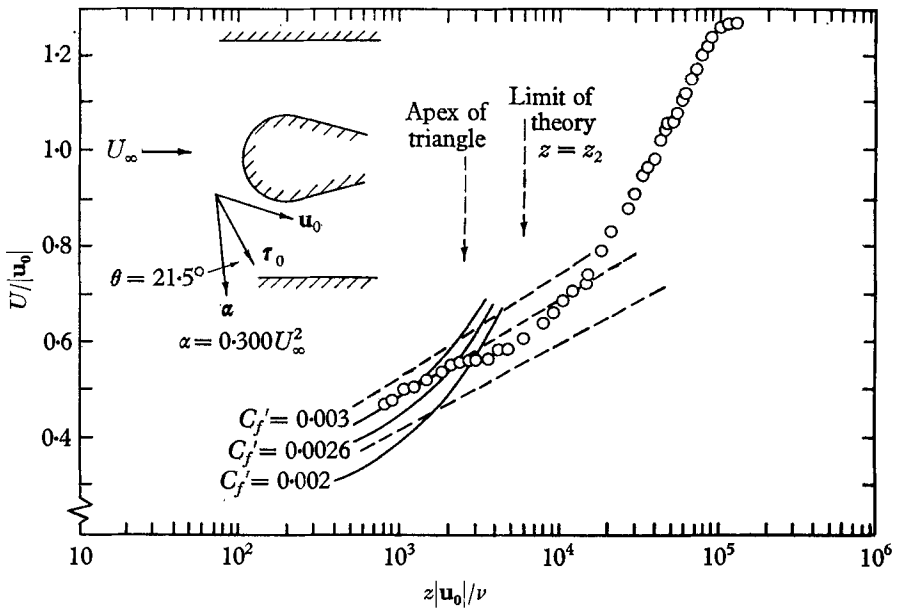

FIGURE 15. Comparison of run 22 with theory. ———, theory; – – – –, Clauser lines.

Plotting of velocity profiles and discussion

For given values of α and θ, a modified Clauser chart can be plotted giving a family of curves for various values of C_f' and the appropriate 'developed' experimental profiles superimposed on this chart to see if it fits this modified scheme. This was done for three profiles. However, the pressure gradients had not been measured very accurately, and so Hornung & Joubert's results for α were assumed to be that given by the potential flow theory around a circular cylinder in an infinite air stream. The experimental profiles are shown in figures 13, 14 and 15.

In figure 13, the results for run 5 are shown and it can be seen that the experimental points follow the Clauser line fairly well but appear to follow the modified theory somewhat better. The maximum possible range over which the theory is valid is not very great but run 5 is fairly close to the separation line and here mean-flow inertia forces could be high. Hornung & Joubert's plot of the wall streamlines show a high curvature near the separation line.

In figure 14 the results of run 14 are shown and here mean-flow inertia forces should be low since the profile is far from the separation line. It can be seen that the experimental points follow the modified theory over a very large range of $z|\mathbf{u}_0|/\nu$. However, they also appear to follow the Clauser line equally well between the same limits.

In figure 15 the results of run 22 are shown. Here mean-flow inertia forces are definitely high since this is very close to the separation line. Also pressure-gradient forces are high. The modified theory follows the experimental points over only a small range. However, an important observation here is that the value of C_f' deduced from the modified theory is considerably different from that which would be deduced from the Clauser line.

All experimental results could be made to fit the theory much better if the value of α was adjusted to fit the large bumps in the plots. However, the variation in α necessary would be a factor of order 2 to 5. In any case, too many degrees of freedom of variables would exist to make any deduction worth while if α was allowed to vary. The results definitely indicate that more accurate measurements of pressure gradient are necessary, while the shear stresses should be measured directly with a hot-wire anemometer. The theory shows some use if only to act as a guide for future research.

REFERENCES

CLAUSER, F. 1954 *J. Aero. Sci.* **21**, 19.
COLES, D. 1956 *J. Fluid Mech.* **1**, 191.
HORNUNG, H. G. & JOUBERT, P. N. 1963 *J. Fluid Mech.* **15**, 368.
JOHNSTON, J. 1960 *Trans. A.S.M.E. Series D*, **82**, 233.
PERRY, A. E. & JOUBERT, P. N. 1963 *J. Fluid Mech.* **17**, 193.
SCHWIND, R. G. 1962 *Gas Turbine Lab., M.I.T. Rep.* no. 67.
TOWNSEND, A. A. 1961 *J. Fluid Mech.* **11**, 97.